INTERNATIONAL JOURNAL FOR NUMERICAL METHODS IN FLUIDS
Int. J. Numer. Meth. Fluids **28**: 1093–1108 (1998)

SYMMETRY TECHNIQUES FOR THE NUMERICAL SOLUTION OF THE 2D EULER EQUATIONS AT IMPERMEABLE BOUNDARIES

ANDREA DADONE*

Istituto di Macchine ed Energetica, Politecnico di Bari, Via Re David 200, 70125 Bari, Italy

SUMMARY

The implementation of boundary conditions at rigid, fixed wall boundaries in inviscid Euler solutions by upwind, finite volume methods is considered. Some current methods are reviewed. Two new boundary condition procedures, denoted as the *symmetry technique* and the *curvature-corrected symmetry technique* are then presented. Their behaviour in relation to the problem of the subsonic flow about blunt and slender elliptic bodies is analysed. The subsonic flow inside the Stanitz elbow is then computed. The *symmetry technique* is proven to be as accurate as one of the current methods, *second-order pressure extrapolation technique*. Finally, for arbitrary curved geometries, dramatic advantages of the *curvature-corrected symmetry technique* over the other methods are shown. © 1998 John Wiley & Sons, Ltd.

KEY WORDS: boundary conditions; Euler equations; finite volume

1. INTRODUCTION

The present paper deals with the implementation of boundary conditions at solid walls in the numerical simulation of compressible inviscid flows governed by the Euler equations. At solid boundaries, in the absence of suction or transpiration, it is generally recognised that the normal velocity component must be set to zero to satisfy the conservation of mass. The pioneering work of Moretti [1] focused on this issue in the early 1960's and described the inadequacies of reflection techniques. As a natural consequence, Moretti and Abbett [2] introduced a characteristic boundary condition, which significantly improved the accuracy of this early computations. Moretti [3] appropriately persevered in this direction with the development of the λ-scheme, widely employed by the present author (see, e.g. Reference [4]). Such a type of characteristic boundary conditions has been applied to non-conservative as well as conservative schemes (see, e.g. References [5,6]).

For finite volume discretisations, only the pressure is required at a solid boundary. Such a pressure can be computed by using the steady state normal momentum equation suggested by Rizzi [7], the simpler extrapolation methods suggested by Walters and Thomas [8], or the characteristic boundary condition suggested by Dadone and Grossman [9]. Such techniques will be reviewed in the next section, with reference to a cell centred scheme.

* Correspondence to: Istituto di Macchine ed Energetica, Politecnico di Bari, Via Re David 200, 70125 Bari, Italy. Tel: + 39 80 5460465; Fax: + 39 80 5460411; E-mail: dadone@imedado.poliba.it

CCC 0271–2091/98/171093–16$17.50

Received March 1997
Revised November 1997

Next we will discuss the *symmetry technique* and the *curvature-corrected symmetry technique*. The *symmetry technique*, strictly valid only for planar walls, is a characteristic type methodology, which was introduced in Reference [10]. It is a physically consistent technique to enforce the impermeability condition at planar walls and mimics the reflection boundary conditions for finite difference methods. The *curvature-corrected symmetry technique* extends the *symmetry technique* to curved walls by taking into account the curvature effects, which may play a meaningful role in determining the computed solution. This method was originally introduced in References [11] and [12], and is applicable to arbitrary curved geometries.

The behaviour of the classical impermeability conditions will be compared with the results obtained by means of the symmetry techniques for the problem of the subsonic flow about blunt and slender elliptic bodies. Dramatic advantages of the *curvature-corrected symmetry technique* over the other methods will be shown. Finally, the subsonic flow inside the Stanitz elbow will be computed and the *curvature-corrected symmetry technique* will be proven to give more accurate results in an internal flow computation too. Moreover, the advantages of the *symmetry technique* will also be outlined.

2. CLASSICAL IMPERMEABILITY CONDITIONS

Consider the Euler equations in a Cartesian co-ordinate system and a semi-discrete finite volume representation of such equations [8]. Our attention is focused on a cell of the computational volume. The flux vector across a cell edge can be expressed as

$$F = [\rho\tilde{v},\ k_x p + \rho u\tilde{v},\ k_y p + \rho v\tilde{v},\ \rho h^o\tilde{v}]^T, \tag{1}$$

where u, v, w are the three components of the velocity vector with respect to the Cartesian co-ordinate system, k_x, k_y are the direction cosines and p, ρ, h^o represent the pressure, the density and the total enthalpy per unit mass, respectively. Finally, $\tilde{v}$ is the velocity component normal to the considered cell edge:

$$\tilde{v} = k_x u + k_y v. \tag{2}$$

If the considered cell edge is located on an impermeable boundary so that $\tilde{v} = 0$, Equation (1) shows that the only quantity required to compute the flux vector at such a cell edge is the pressure at the wall.

The surface pressure can be extrapolated from the interior of the flow field. One approach is to extrapolate such a pressure so that the normal momentum equation is satisfied [7]. This condition requires that the derivative of the pressure at the wall taken along its normal (n) is given by

$$\left(\frac{\partial p}{\partial n}\right)_{\mathrm{w}} = -\frac{\rho}{R}\tilde{u}^2, \tag{3}$$

where R is the radius of curvature of the wall, subscript w refers to the wall, and $\tilde{u}$ is the velocity component tangential to the body:

$$\tilde{u} = k_y u - k_x v. \tag{4}$$

For orthogonal grids, Equation (3) has been discretised in Reference [7] as (normal momentum pressure extrapolation)

$$p_w = p_1 - \rho_1 \frac{\tilde{u}_1^2}{R} \Delta n_1, \tag{5}$$

where the subscript 1 refers to the cell centre nearest to the body and Δn_1 indicates its distance from the body. More often, the value of the surface pressure is taken as the value at the nearest cell centre [8] (first-order pressure extrapolation):

$$p_w = p_1. \tag{6}$$

The surface pressure can be obtained more accurately by means of a linear extrapolation from the two nearest cell centres [8] (second-order pressure extrapolation):

$$p_w = 1.5p_1 - 0.5p_2, \tag{7}$$

where subscripts 1 and 2 refer to such cell centres.

These three extrapolation techniques can result with a possible inconsistency when computing supersonic flow problems with embedded oblique shocks, since such a shock may lie between the surface and the nearest cell centres, even in the limit of vanishing cell size. Consequently, an alternative characteristic boundary condition has been suggested in Reference [9], which leads to the relation

$$p_w = p_1 \pm \rho_1 a_1 \tilde{v}_1, \tag{8}$$

where a is the speed of sound and $\tilde{v}$ is the velocity component normal to the wall. Moreover, the plus and minus signs apply to lower and upper walls, respectively.

3. CURVATURE CORRECTED SYMMETRY TECHNIQUE

It is well known that numerical schemes lose accuracy where some change is inserted. Variations in the numerical scheme can generally be found at the boundaries, because of the lack of some numerical information. Obviously, such variations also take place at solid walls. In order to restore the original numerical accuracy, the wall boundary discontinuity must be eliminated, which may be accomplished by inserting two extra rows of cells outside the computational flow field. The fluid dynamic variables at the corresponding cell centres must warrant the impermeability condition at the wall. Such a condition is not sufficient to completely define the values of such variables, so that a model of the flow field in the wall vicinity is needed. The most appropriate model is represented by a vortex flow of constant entropy and total enthalpy, which satisfies the normal momentum equation (Equation (3)). The proposed *curvature-corrected symmetry technique* is based on the previous analysis: two extra rows of cells, an appropriate vortex flow, and the enforcement of the impermeability condition at the wall.

As shown in Figure 1, two image cells are located below the surface of the wall in a symmetric position with respect to the internal cells. At the corresponding image cell centres, the fluid dynamic conditions are evaluated as follows. In the vicinity of the wall, the velocity component normal to the wall is generally small enough to be considered equal to zero. Accordingly, the pressure values at the two image points (refer to Figure 1) can be determined from an integration of Equation (3), which can be approximated in the same spirit of Equation (5):

$$p_{-i} = p_i - 2\rho_1 \frac{\tilde{u}_1^2}{R} \Delta n_i, \tag{9}$$

where the subscript i is equal to 1 or 2, and Δn_i indicates the distance between the cell centre (i) and the wall.

Two other flow conditions may be evaluated by locally modelling the inviscid flow as a vortex flow of constant entropy and total enthalpy, i.e. by assuming symmetric values of such quantities. Such a condition leads to

$$\rho_{-i} = \rho_i \left(\frac{p_{-i}}{p_i} \right)^{1/\gamma}, \qquad \tilde{u}^2_{-i} = \tilde{u}^2_i + \frac{2\gamma}{\gamma - 1} \left(\frac{p_i}{\rho_i} - \frac{p_{-i}}{\rho_{-i}} \right) + \tilde{v}^2_i - \tilde{v}^2_{-i}, \tag{10}$$

where the subscript i is equal to 1 or 2 and γ is the constant ratio of specific heats.

The remaining condition stems from the impermeability condition. In the computed results, the finite volume flux-difference splitting method which uses the approximate Riemann solver due to Roe [13] will be used. As a consequence, the impermeability condition is enforced by assigning an antisymmetric value to $\tilde{v}_{-1}$ and by selecting $\tilde{v}_{-2}$ in such a way that the Roe averaged value of the normal velocity component $\tilde{v}$ is zero at the surface. In the absence of limiters, using linear extrapolations for the left and right states, these conditions imply

$$\tilde{v}_{-1} = -\tilde{v}_1, \qquad \tilde{v}_{-2} = 3\tilde{v}_{-1} + 2[\tilde{v}_1 + (\tilde{v}_1 - \tilde{v}_2)/2] \sqrt{\frac{\rho_1 + (\rho_1 - \rho_2)/2}{\rho_{-1} + (\rho_{-1} - \rho_{-2})/2}}. \tag{11}$$

The present methodology presents several advantages. Firstly, the surface flux evaluation procedure is consistent with the flux evaluation technique employed at the internal cell edges. Moreover, the present procedure allows second-order spatial accuracy for both the surface cell edge and the first cell edge off the surface. As a consequence, no change in the numerical scheme is required at the wall, so that a limited entropy generation can be expected. Finally, limiters can be implemented, as with any internal cell edge flux evaluation.

Equations (9)–(11) completely define the flow conditions at the image points (-1) and (-2), while no fluid dynamic variable is defined at the wall surface. On the contrary, the classical impermeability conditions, Equations (5)–(8), define the wall pressure, which is required for data presentation purposes. The *curvature-corrected symmetry technique* uses the Roe approximate Riemann solver as a mean to evaluate the wall fluxes, from which a pressure value could be computed. Such a value does not accurately represent the surface pressure, because of the method used in the application of the Riemann solution for the evaluation of the surface flux. This flux is computed from discontinuous left and right states of the flow variables at a cell edge. The value of the surface flux from the Riemann solver, although appropriate for the time integration of the solution for the cell-averaged conserved variables, does not accurately represent the surface pressure. As a consequence, the *curvature-corrected symmetry technique* has a second part, which involves the computation of the physical wall

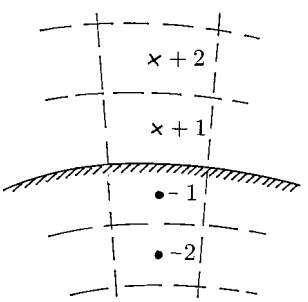

Figure 1. Image cells for symmetry techniques.

pressure, useful only for data presentation purposes: when the converged solution has been obtained, the surface pressure is extrapolated from interior cell centre values consistently with the normal momentum equation evaluated at the surface, Equation (3):

$$p_w = \left[p_1 \Delta n_2^2 - p_2 \Delta n_1^2 - \rho_w \frac{\tilde{u}_w^2}{R} \Delta n_1 \Delta n_2 (\Delta n_2 - \Delta n_1) \right] / (\Delta n_2^2 - \Delta n_1^2). \tag{12}$$

When applying Equation (12), the values of density and velocity at the wall have been taken as equal to the values of the corresponding variables at the nearest cell centre (1). This avoids extrapolations across discontinuities and has a minimal effect on the results. This second part of the *curvature-corrected symmetry technique*, as already stated, is only useful for data presentation purposes and does not influence the computation itself, which uses only the first part of the outlined technique.

4. SYMMETRY TECHNIQUE

When planar walls are considered or when curved walls are locally approximated by flat plates, $R \to \infty$, so that a simplified technique may be devised. Such a simplified technique has been named *symmetry technique*. It is strictly valid only for steady flows over planar walls, although it may be used as an approximate technique for curved walls. Owing to the condition $R \to \infty$, Equations (9)–(11) may be simplified, so that the pressure, the density and the velocity components at the two image cells located below the surface (Figure 1) are given by

$$\begin{aligned} p_{-1} &= +p_1, \quad p_{-2} = +p_2, \\ \rho_{-1} &= +\rho_1, \quad \rho_{-2} = +\rho_2, \\ \tilde{u}_{-1} &= +\tilde{u}_1, \quad \tilde{u}_{-2} = +\tilde{u}_2, \\ \tilde{v}_{-1} &= -\tilde{v}_1, \quad \tilde{v}_{-2} = -\tilde{v}_2. \end{aligned} \tag{13}$$

Similarly to the *curvature-corrected symmetry technique*, the second part of this boundary condition technique involves the computation of the physical wall pressure by means of Equation (12). Again, it should be noted that this surface pressure is only used for presentation purposes and does not influence the computation itself, which uses only the first part of the outlined technique.

Equation (13) outlines that the pressure, the density and the velocity vector at the two image cell centres are taken symmetrically from their counterparts in the interior of the computational domain. Such a situation has determined the definition of the methodology as the *symmetry technique*. Moreover, such a symmetry of Equation (13) warrants that the following physical property is preserved. If we consider a full plane problem which presents a symmetric solution with respect to a symmetry axis, the computation can be extended only to the half plane delimited by the symmetry axis. At such a straight line, the normal velocity component must be zero, because of the symmetry. As a consequence, in the half plane problem the symmetry axis is represented by a planar wall. Obviously, the full and half plane problems should give exactly the same results. Such a physical condition is satisfied if the *symmetry technique* is used, while it is only approximately satisfied if any one of the classical impermeability conditions is used.

In the absence of any flux limitation, the approximate Riemann solver due to Roe [13] gives the following relation for the wall pressure used to compute the surface flux:

$$p_w = p_r + \rho_r \tilde{v}_r [\tilde{v}_r - a_w], \tag{14}$$

where subscript r refers to the right state, obtained by means of an appropriate MUSCL extrapolation. Moreover, $a_w^2 = (\gamma - 1)(H_r - \tilde{u}_r^2/2)$, where H is the total enthalpy. Comparison of Equation (14) with (8) indicates that this relationship can be considered as a characteristic boundary condition within the framework of Roe's method. Accordingly, the *symmetry technique* must be considered as a characteristic boundary condition.

Finally it must be remarked that the *symmetry technique* coincides with the boundary condition at planar walls used in connection with the λ-scheme, as already proven in Reference [10].

5. RESULTS

5.1. Elliptic body

Two-dimensional subsonic flows about a blunt and a slender elliptic body are analysed here to test the accuracy of the *symmetry techniques* in comparison with the other reviewed procedures. Three different O-grids made by 32×8, 64×16, and 128×32 cells have been employed, the higher number of cells being located in the circumferential direction.

First, a blunt elliptic body, with an axis ratio equal to 0.75, has been considered. The circular farfield boundary was located at 17.5 times the major axis dimension. The undisturbed Mach number, equal to 0.30, causes a maximum Mach number close to 0.82 to take place on the ellipse surface. Computations have been performed using the second-order (P-II) and the normal momentum (NME) pressure extrapolation, along with the symmetry (ST) and the curvature-corrected symmetry (CCST) techniques.

Many different parameters have been considered in order to compare the effectiveness of the different boundary condition methods. The leading edge pressure, p_{le}, divided by the total pressure, $p°$, is plotted in Figure 2(a) versus the inverse of the total number of cells, N. From these results, it appears that all the methods are consistent and approach the exact value, equal to 1, in the limit of a vanishing cell size. The CCST results, however, appear to be significantly more accurate than those computed with the other approaches. Other results confirming the remarkable behaviour of the CCST are plotted in Figure 2(b–d): the trailing edge pressure, p_{te}, is reported in Figure 2(b); the L_2 norm of the total pressure error on the surface of the body is represented in Figure 2(c); the drag coefficient, C_d, is shown in Figure 2(d). In particular, Figure 2(b) confirms the grid convergence of the CCST but also shows the improved accuracy of this method even at the fine grid level: the ST, P-II and NME have about a 1% error in trailing edge pressure, while in stark contrast the CCST shows a remarkable 0.1% error.

Next, the Mach number and the entropy contours are presented in Figures 3 and 4. The computations were performed by employing the finest 128×32 grid. The Mach number contours are spaced at $\Delta M = 0.1$ and the entropy contours are spaced at $\Delta s = 0.001$. A remarkable Mach number contour symmetry can be observed for the CCST, while a significant asymmetry is caused by the P-II. Moreover, the P-II generates high spurious entropy levels ($s_{max} = 0.0067$), while the CCST causes minute values of spurious entropy ($s_{max} = 0.0009$). The other technique results are not reported for the sake of conciseness and do not alter the previous conclusions: the ST gives results slightly better than the P-II; the NME gives results very close to the P-II, concerning the Mach contours, and the worst results in relation to the entropy contours. In particular, $s_{max} = 0.0059$ for the ST and $s_{max} = 0.0114$ for the NME.

A slender elliptic body, with an axis ratio equal to 0.125, was then considered. The circular farfield boundary is located at 10.5 times the major axis dimension. The undisturbed Mach number, equal to 0.75, causes a maximum Mach number close to 0.94 to take place on the ellipse surface. Computations were performed using the previous four techniques. Only the leading edge pressure (Figure 5(a)) and the trailing edge pressure (Figure 5(b)) are presented. A quick glance to such figures allows confirmation of the conclusions drawn from Figure 2(a–d). Moreover, Figures 6 and 7 present the Mach number contours obtained by means of the P-II and the CCST, respectively. The asymmetry of the P-II results is less evident in the present case, although the distortion in the wake region indicates the presence of spurious

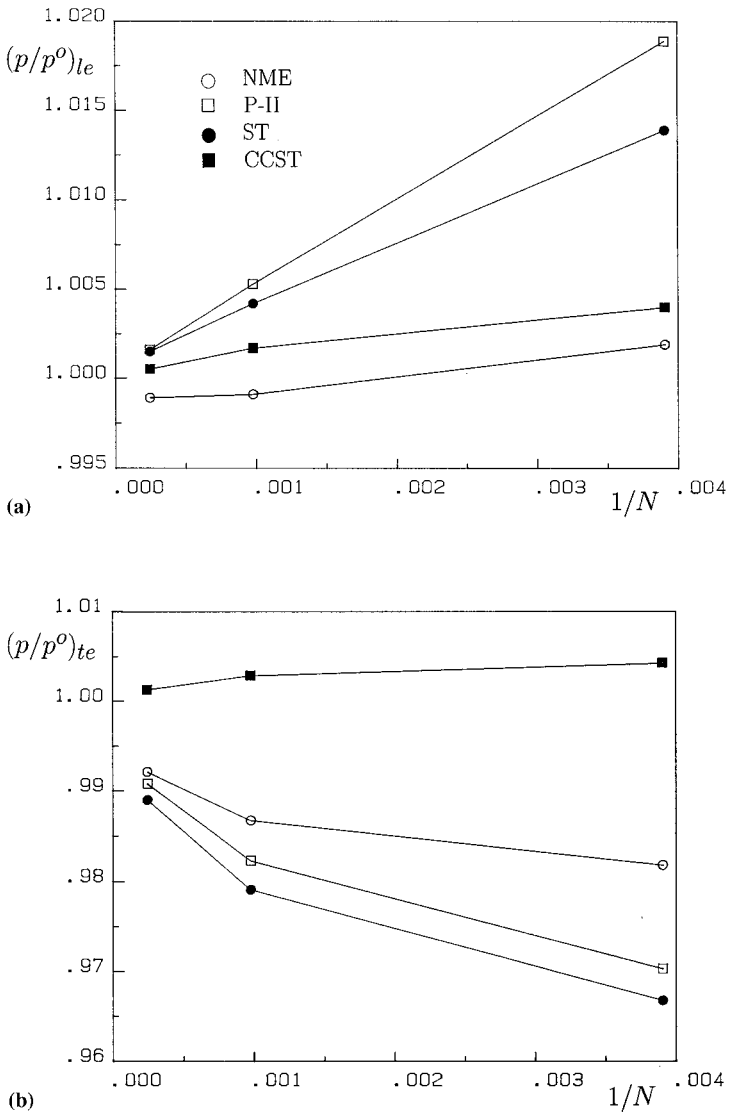

Figure 2. (a) Leading edge pressure—blunt elliptic body; (b) trailing edge pressure—blunt elliptic body; (c) L_2-norm surface total pressure error—blunt elliptic body; (d) drag coefficient—blunt elliptic body.

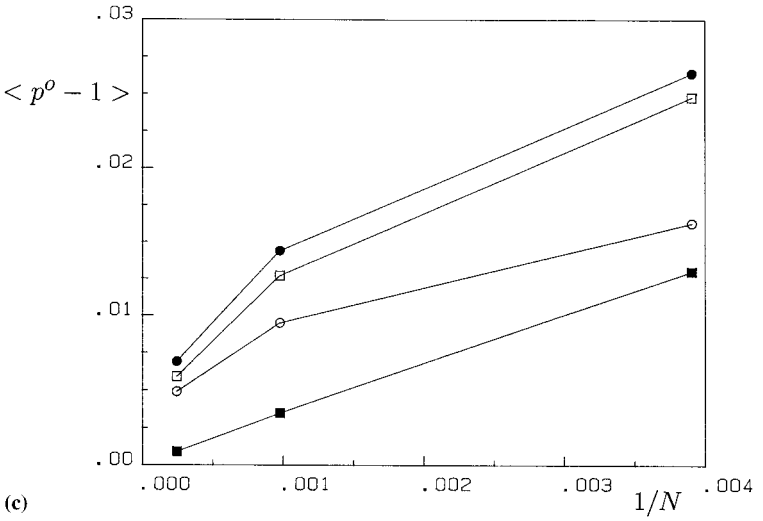

(c)

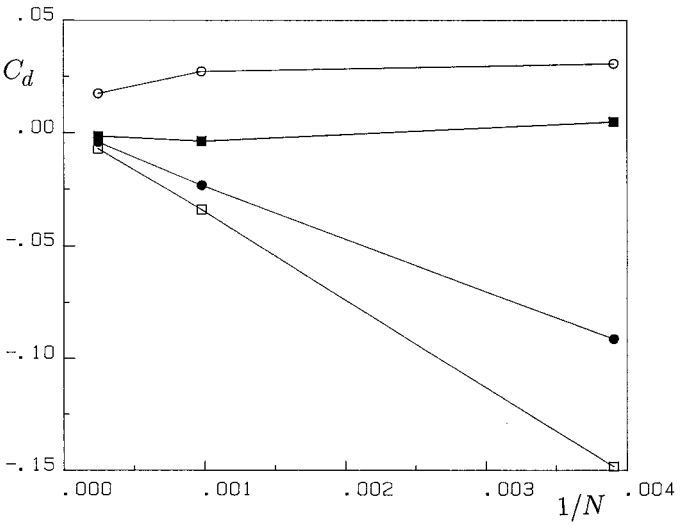

(d)

Figure 2 (*Continued*)

entropy levels. Indeed the entropy contours, not presented here, confirm such a spurious entropy generation: $s_{\max} = 0.0065$ for the P-II, while it reduces to 0.0015 for the CCST. Also in the present test case, the NME causes the worst entropy generation: $s_{\max} = 0.0174$.

All of the previous computations were also performed by employing the first-order pressure extrapolation technique. The corresponding results are not here reported for the sake of figure clarity. Nevertheless, it is worth mentioning that all of them show a very poor accuracy.

5.2. Stanitz elbow

A more practical flow case is considered here, namely the subsonic flow inside the Stanitz elbow [14]. The duct geometry is two-dimensional, although appropriate inlet conditions can

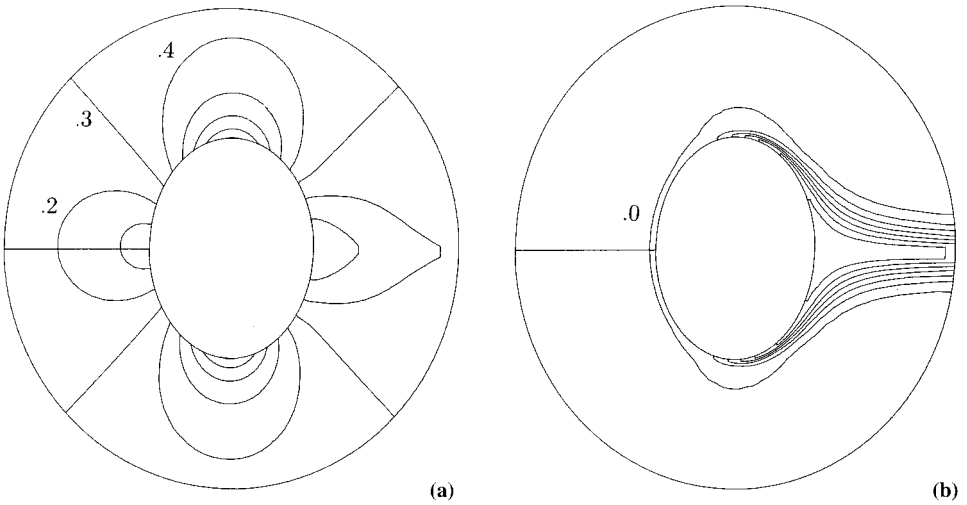

Figure 3. (a) Mach number contours—blunt elliptic body: second-order pressure extrapolation P-II; (b) entropy contours—blunt elliptic body: second-order pressure extrapolation P-II.

produce a three-dimensional flow in the elbow. In the present computation a two-dimensional flow condition was considered, corresponding to a nominal main stream exit Mach number equal to 0.8. Computations were performed using the second-order (P-II) and the normal momentum (NME) pressure extrapolation, along with the symmetry techniques (ST and CCST). Three different grids made by 16×8, 32×16, and 64×32 cells have been employed, the higher number of cells being located in the streamwise direction. The duct geometry and the intermediate employed mesh are shown in Figure 8.

The pressure distributions on the pressure and suction surfaces are plotted in Figure 9(a). The abscissa is the curvilinear co-ordinate, ξ, adimensionalized with respect to the curvilinear

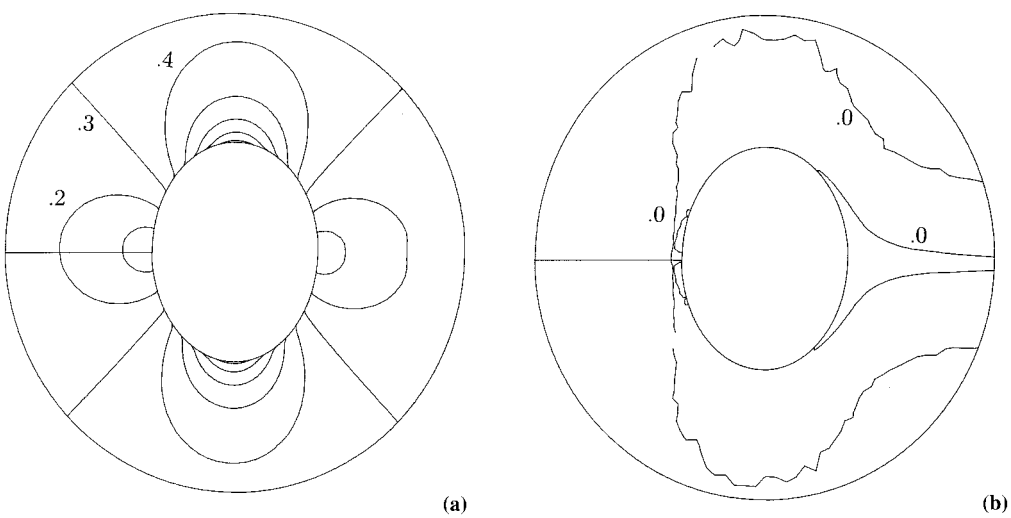

Figure 4. (a) Mach number contours—blunt elliptic body: curvature corrected symmetry technique CCST; (b) entropy contours—blunt elliptic body: curvature corrected symmetry technique CCST.

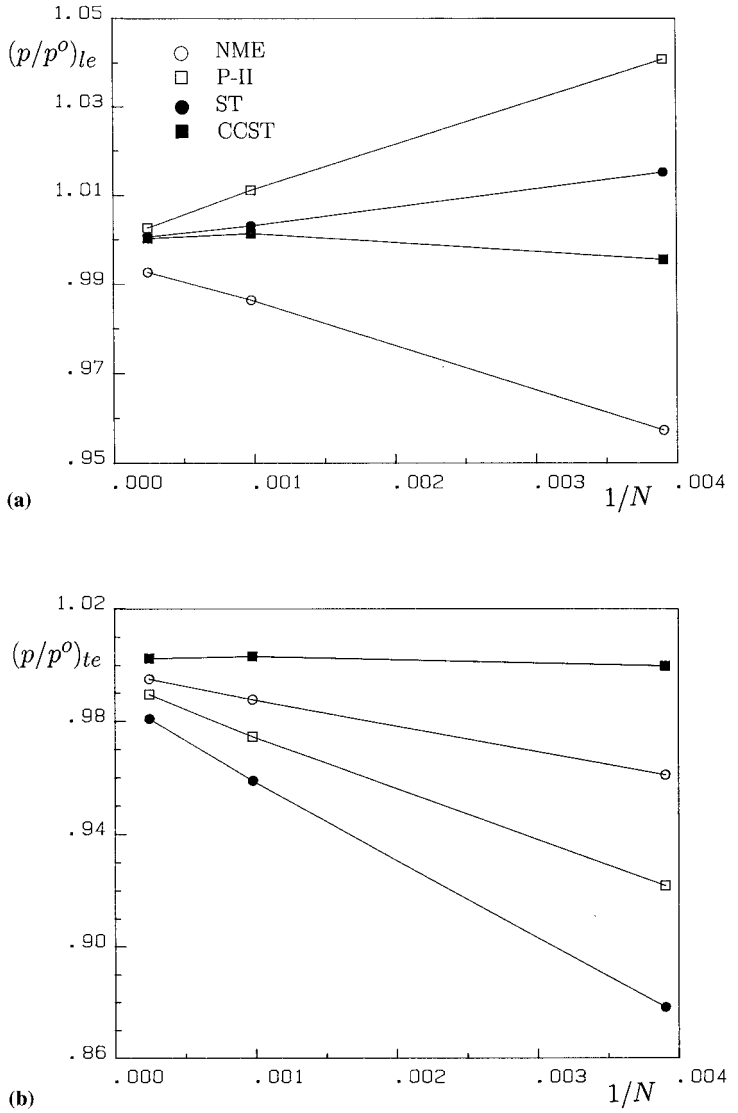

Figure 5. (a) Leading edge pressure—slender elliptic body; (b) trailing edge pressure—slender elliptic body.

distance, ξ_l, between the inlet and the outlet sections. The results of Figure 9(a) refer to the finest employed grid and were computed using the four different techniques. A quick glance to such a figure shows that the four techniques predict practically coincident results, with minor differences on the suction surface at intermediate ξ values. The pressure distributions on the suction surface at $\xi/\xi_l = 0.4 \div 0.5$ are plotted in Figure 9(b,c). The results in Figure 9(b) were computed using the intermediate grid (32×16), while Figure 9(c) refers to the coarsest grid (16×8). The continuous line in these figures represents the mesh converged solution. Figure 9 again proves that all the methods are consistent and tend to approach the same distribution in the limit of a vanishing cell size. However, the CCST results appear to be significantly more accurate than the other approaches. Indeed, the intermediate mesh results practically coincide

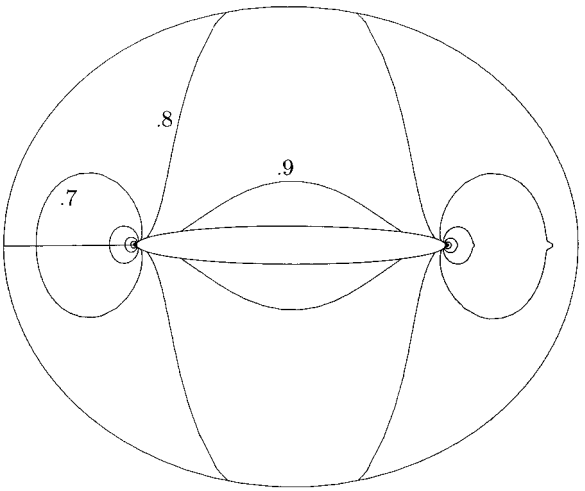

Figure 6. Mach number contours—slender elliptic body: second-order pressure extrapolation P-II.

with the mesh converged ones, and also the coarsest mesh results show a reasonable agreement. Moreover, the ST and P-II results are practically coincident, and the NME results rank second in terms of accuracy.

The Mach number distributions are plotted in Figure 10. Figure 10(a) refers to the finest grid, Figure 10(b) to the intermediate one and Figure 10(c) to the coarsest grid. All the previous conclusions can again be drawn: all the results are practically coincident at the finest mesh level; all the methods are consistent; the CCST results are undoubtedly more accurate; the CCST intermediate mesh results practically coincide with the mesh converged ones; the ST and P-II results are practically coincident; the NME results rank second in terms of accuracy.

The first-order pressure extrapolation technique was also employed for the present computations. The corresponding results, not reported here, again showed the poorest accuracy.

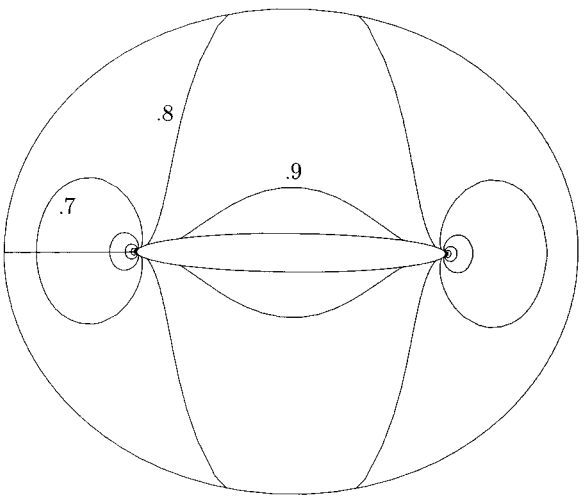

Figure 7. Mach number contours—slender elliptic body: curvature corrected symmetry technique CCST.

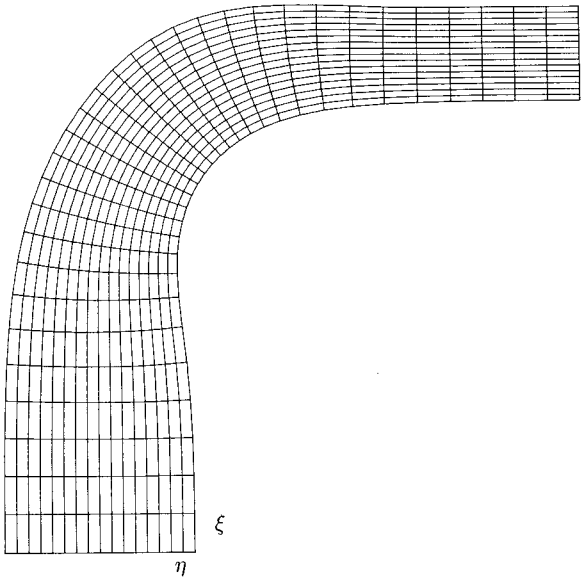

Figure 8. Duct geometry and intermediate mesh—Stanitz elbow.

As far as the efficiency is concerned, all the employed methodologies require approximately the same number of iterations to obtain a converged solution. In particular, the NME and CCST techniques have shown to be slightly more efficient, although the differences are relatively small.

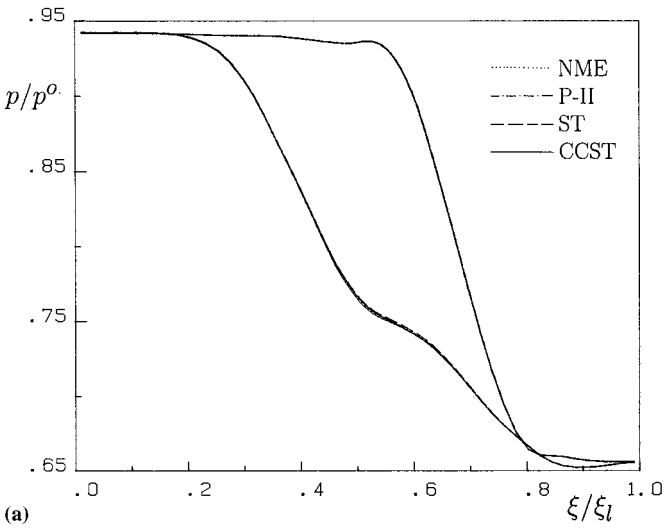

Figure 9. (a) Pressure distribution on suction and pressure surfaces—Stanitz elbow: 64×32 cells; (b) pressure distribution on suction surface—Stanitz elbow: 32×16 cells; (c) pressure distribution on suction surface—Stanitz elbow: 16×8 cells.

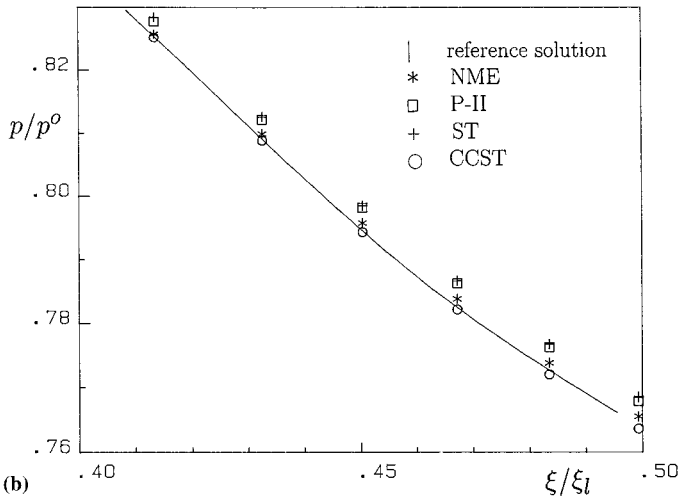

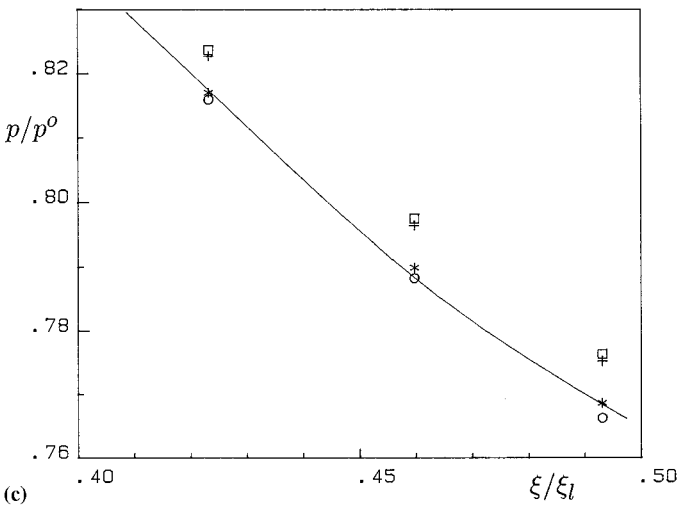

Figure 9 (*Continued*)

6. CONCLUSIONS

Classical techniques used to enforce the impermeability condition at rigid, fixed wall boundaries have been outlined. The *symmetry technique*, quite appropriate to enforce the impermeability condition at a plane wall, has been presented, together with the *curvature-corrected symmetry technique*, which is more appropriate for a curved wall.

The *curvature-corrected symmetry technique* was used to compute two simple two-dimensional subsonic flow test cases, i.e. the flow about a blunt and a slender elliptic body. The computed results were compared with those obtained by means of other techniques. The suggested technique gives more accurate results: the computational errors are reduced by one order of magnitude, the isoMach patterns are quite symmetric between the front and rear portion, the isoentropy patterns show entropy levels quite close to zero.

Finally, the subsonic flow in a contracting curved duct was computed and again, the results established the superior accuracy of the *curvature-corrected symmetry technique*. Indeed, accurate results have been computed using much coarser grids.

All of the computed results have also proven that the *symmetry technique* and the second-order pressure extrapolation technique are characterised by almost the same accuracy, and that the normal momentum pressure extrapolation causes an excessive entropy generation at the walls, when the computed flow case involves a stagnation point, while it gives a better accuracy for flows in curved ducts. Finally, the first-order pressure extrapolation technique gives the poorest accuracy. The poor quality of these results must be remarked because many

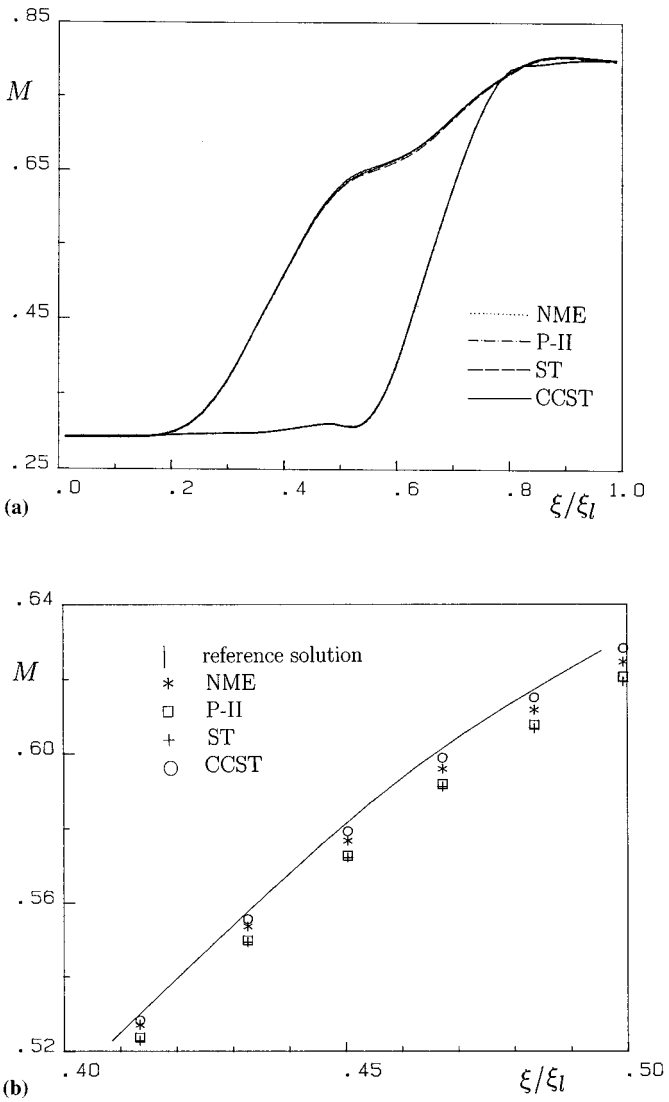

Figure 10. (a) Mach number distribution on suction and pressure surfaces—Stanitz elbow: 64×32 cells; (b) Mach number distribution on suction surface—Stanitz elbow: 32×16 cells; (c) Mach number distribution on suction surface—Stanitz elbow: 16×8 cells.

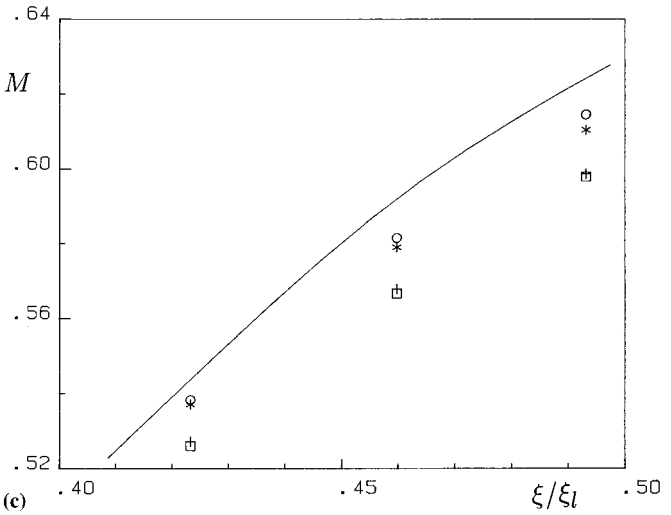

Figure 10 (*Continued*)

cell-centred, upwind finite volume codes use such a technique for robustness, because it does not require any extrapolation, which may be troublesome in presence of oblique shocks located close to the wall. It is the author's opinion that the *symmetry technique* and the *curvature-corrected symmetry technique* are as robust as the first-order pressure extrapolation technique and much more robust than the second-order pressure extrapolation technique. At least, this is certainly true for the *symmetry technique*, so that its use should be recommended if the *curvature-corrected symmetry technique* is not considered robust enough.

Moreover, it must be remarked that it is very simple to implement the suggested techniques in existing codes, they require almost no extra computational effort, and the code efficiency is not impaired.

Recent studies have addressed the extension of the *curvature-corrected symmetry techniques* to three-dimensional flows. Preliminary results indicate that it may be easily extended by applying the two-dimensional methodology in the osculating plane. Finally, it must be remarked that all the considered techniques are apt to compute steady flows.

ACKNOWLEDGMENTS

The present research has been supported by the Italian Agency MURST (Ministero dell'Universitá e della Ricerca Scientifica e Tecnologica). The author acknowledges a journal reviewer for many important and helpful suggestions.

REFERENCES

1. G. Moretti, 'Importance of boundary conditions in the numerical treatment of hyperbolic equations', *High Speed Comput. Fluid Dyn., Phys. Fluids*, Supplement II, 13–20 (1969).
2. G. Moretti and M. Abbett, 'A time-dependent computational method for blunt body flows', *AIAA J.*, **4**, 2136–2141 (1966).
3. G. Moretti, 'The λ-scheme', *Comput. Fluids*, **7**, 191–205 (1979).
4. A. Dadone and G. Moretti, 'Fast Euler solver for transonic airfoils', *AIAA J.*, **26**, 409–425 (1988).
5. S.R. Chakravarthy, 'Euler equations-implicit schemes and boundary conditions', *AIAA J.*, **21**, 699–706 (1983).

6. D.L. Marcum and J.D. Hoffman, 'Numerical boundary condition procedure for Euler solvers', *AIAA J.*, **25**, 1054–1068 (1987).
7. A. Rizzi, 'Numerical implementation of solid boundary conditions for the Euler equations', *Z.A.M.M.*, **58**, T301–T304 (1978).
8. R.W. Walters and J.L. Thomas, 'Advances in upwind relaxation methods', in A.K. Noor (ed.), *State-of-the-Art Surveys of Computational Mechanics*, Ch. 4, ASME publication, 1988.
9. A. Dadone and B. Grossman, 'Characteristic-based, rotated upwind scheme for the Euler equations', *AIAA J.*, **30**, 2219–2226 (1992).
10. A. Dadone, 'A physical numerical treatment of impermeable boundaries in compressible flow problems', *Proc. 4th Int. Symp. Comp. Fluid Dyn.*, Davis, CA, **1**, 258–263 (1991).
11. A. Dadone, 'A numerical technique to compute Euler flows at impermeable boundaries based on physical considerations', *Notes Numer. Fluid Dyn.*, **43**, 171–178 (1993).
12. A. Dadone and B. Grossman, 'Surface boundary conditions for the numerical solution of the Euler equations', *AIAA Paper 93-3334-CP* (1993). Also, *AIAA J.*, **32**, 285–293 (1994).
13. P.L. Roe, 'Characteristic-based schemes for the Euler equations', *Annu. Rev. Fluid Mech.*, **18**, 337–365 (1986).
14. J.D. Stanitz, 'Design of 2-D channels with prescribed velocity distributions along the channel walls, I—Relaxation Solutions', *NACA TN 2593* (1952).

